INTERNATIONAL JOURNAL FOR NUMERICAL METHODS IN FLUIDS, VOL. 24, 493–517 (1997)

VISCOELASTIC MODELLING OF ENTRANCE FLOW USING MULTIMODE LEONOV MODEL

MAHESH GUPTA

Department of Mechanical Engineering and Engineering Mechanics, Michigan Technological University, Houghton, MI 49931, U.S.A.

AND

C. A. HIEBER AND K. K. WANG

Sibley School of Mechanical and Aerospace Engineering, Cornell University, Ithaca, NY 14853, U.S.A.

SUMMARY

A simulation of planar 2D flow of a viscoelastic fluid employing the Leonov constitutive equation has been presented. Triangular finite elements with lower-order interpolations have been employed for velocity and pressure as well as the extra stress tensor arising from the constitutive equation. A generalized Lesaint–Raviart method has been used for an upwind discretization of the material derivative of the extra stress tensor in the constitutive equation. The upwind scheme has been further strengthened in our code by also introducing a non-consistent streamline upwind Petrov–Galerkin method to modify the weighting function of the material derivative term in the variational form of the constitutive equation. A variational equation for configurational incompressibility of the Leonov model has also been satisfied explicitly.

The corresponding software has been used to simulate planar 2D entrance flow for a 4:1 abrupt contraction up to a Deborah number of 670 (Weissenberg number of 6·71) for a rubber compound using a three-mode Leonov model. The predicted entrance loss is found to be in good agreement with experimental results from the literature. Corresponding comparisons for a commercial-grade polystyrene, however, indicate that the predicted entrance loss is low by a factor of about four, indicating a need for further investigation.

KEY WORDS: viscoelasticity; Leonov model; entrance flow; upwind scheme; polymer; rheology

1. INTRODUCTION

For numerical simulation of the flow of polymeric fluids, a purely viscous but shear-thinning rheological behaviour has been successfully used in many applications involving shear-dominated flows, such as in the injection and compression moulding of polymers. However, in applications involving extensional flow, predictions from such a simple formulation can be quite different from the real flow. Owing to their viscoelastic nature, polymers accumulate significant recoverable strain. This recoverable strain is the main reason for the poor prediction of extension-dominated polymeric flows by a purely viscous formulation. One such flow involving significant extension, which has been used extensively as a test case in the literature, is entrance flow. Besides being a good test case, entrance flow is frequently encountered in polymer-processing applications. For instance, the runner and gate system in injection moulding and the die portion in extruders involve channels with a contraction and/or expansion in cross-sectional area.

CCC 0271–2091/97/050493–25

Received 27 July 1995
Revised 26 June 1996

To capture the viscoelastic behaviour of polymers, many different constitutive equations have been proposed in the literature. A good review of such equations can be found in the book by Larson.[1] The constitutive equation given by Leonov[2] has been used in the present work. This equation has been employed by many other investigators[3–6] and has been found to be capable of predicting complex polymeric flows.

Numerical simulation of viscoelastic flows has been actively investigated by researchers for quite some time. A good review on the subject is presented by Keunings.[7] Many of the numerical schemes developed in the literature successfully simulated viscoelastic flows at low strain rates but failed to converge at higher strain rates of practical interest. Significant progress has been made in the last decade towards identification of underlying causes for early divergence of the simulation and towards development of stable numerical techniques. Joseph *et al.*[8] showed that equations governing two-dimensional steady flow of Maxwell fluids have two imaginary characteristics and that streamlines correspond to two real characteristics. Besides these four characteristics, the upper-convected Maxwell model has two more characteristics associated with the vorticity equation which, depending upon the sign of the determinant of the Finger tensor ($\det \tilde{c}$), can be real ($\det \tilde{c} > 0$) or imaginary ($\det \tilde{c} < 0$). Dupret and Marchal[9] showed for the upper-convected Maxwell fluid that if the Finger tensor is positive definite at the inlet boundaries, then it will remain positive definite everywhere in the flow domain. Thus the upper-convected Maxwell model is always evolutionary. For the Oldroyd-B fluid, which has an additional Newtonian viscosity (or retardation time), Dupret and Marchal[9] showed that the Finger tensor is always positive definite and that neither change in type nor loss of evolution can occur. For the Leonov model the Finger tensor is positive definite by definition. Leonov[10] showed that the Leonov model based on the rubber elasticity work potential is globally evolutionary.

In a purely viscous incompressible flow the constitutive equation can be used to eliminate the stress variable, leaving only velocity and pressure in the governing equations; however, such an explicit elimination of the stress tensor is typically not feasible in the case of viscoelastic constitutive equations. For the simulation of a purely viscous incompressible flow in terms of a velocity–pressure formulation based on the finite element method, the velocity and pressure interpolations must satisfy the Babuska–Brezzi compatibility condition.[11,12] It was shown by Fortin and Pierre[13] that if the space of the velocity gradient is a subset of the solution space of the extra stress tensor, then the compatibility condition for the velocity–pressure–stress formulation is the same as the Babuska–Brezzi condition. However, the velocity gradient in the finite element method is typically discontinuous across the element boundary and will not be a subset of the solution space of the extra stress tensor if continuous interpolations are used for the extra stress. In order to approximate the compatibility condition for the velocity–pressure–stress formulation, Marchal and Crochet[14] discretized the velocity and pressure only, leaving the extra stress tensor undiscretized in the variational equations. To satisfy the compatibility condition approximately, Marchal and Crochet divided each quadrilateral element into n^2 uniform subelements, expecting the condition to be approximated closely for large n. For Newtonian fluids, with $n = 4$ (16 subelements), Marchal and Crochet obtained results similar to those from the velocity–pressure formulation. It was shown by Fortin and Pierre[13] that the error estimate for the mixed method of Marchal and Crochet is of optimal order.

Since viscoelastic constitutive equations typically constitute a set of first-order hyperbolic equations, an upwind scheme is usually required in order to obtain a stable numerical scheme. Various upwind schemes have been proposed in the literature. Upadhyay and Isayev[3] integrated the Leonov constitutive equation along streamlines to calculate the extra stress due to the recoverable portion of the Finger tensor. Velocity and pressure in this scheme were determined by solving the Stokes flow equations with the extra stress term treated as a body force. Upadhyay and Isayev presented results up to a Deborah number of 50 for a 2 : 1 planar entrance flow. The scheme has been used more recently by Hulsen and Zanden[5] and Isayev and Huang[6] for simulations with Giesekus

(axisymmetric) and Leonov (planar) models respectively, where results at higher Deborah numbers have been obtained for a 4 : 1 entrance flow (up to 256 by Hulsen and Zanden and 846 by Isayev and Huang). Recirculation zones, which are found in many such flows of interest, cannot be handled directly by this scheme. Accordingly, different approaches have been used by Upadhyay and Isayev[3] and Hulsen and Zanden[5] to circumvent this difficulty. As an alternative, the streamline upwind Petrov–Galerkin (SUPG) method developed by Brooks and Hughes[15] modifies the weighting function in the variational form of the constitutive equation so as to give higher weight to points on the upwind side of the finite element. Marchal and Crochet[14] used a non-consistent streamline upwind (SU) method in which the weighting function in the variational form of the constitutive equation is modified for the convection term only, whereas the weighting function for other terms in the constitutive equation is the same as that in the conventional Galerkin method. Marchal and Crochet observed some oscillations in the velocity and stress field obtained with the SUPG method, whereas the corresponding distributions obtained by using the SU method were found to be smooth. Luo and Tanner[16] also confirmed superior convergence properties of the SU method over the conventional Galerkin as well as the SUPG method. However, in a one-dimensional study with a sinusoidal forcing function, Tanner and Jin[17] found the SU scheme to be less accurate than the SUPG as well as the conventional Galerkin method.

Taking advantage of the discontinuous discretization of the extra stress tensor, which is required to satisfy the compatibility condition, Fortin and Fortin[18] and Fortin and Zine[19] have used the method of Lesaint and Raviart[20] for upwind discretization of the convection term. In this approach an extra surface integral term is added in the variational form of the constitutive equation. This surface integral term vanishes if the interpolation is continuous across the element boundary; however, for discontinuous discretization of the extra stress tensor, the surface integral term incorporates some upwinding in the variation of the convection term. The Lesaint–Raviart method has also been used by Basombrio *et al.*[21] and Baaijens,[22] who both used triangular finite elements instead of the quadrilateral element employed by Fortin.

In the present work a triangular finite element is used with quadratic and linear (enriched by a constant) interpolations for velocity and pressure respectively. This combination of velocity and pressure interpolation not only satisfies the Babuska–Brezzi condition but also guarantees local mass balance over each finite element.[23] To satisfy the compatibility condition for the velocity–pressure–stress formulation, we have employed a linear discontinuous (across the finite element boundaries) interpolation for the extra stress tensor. A generalized Lesaint–Raviart (GLR) method, described in the next section, has been used for upwind discretization of the convection term. Upwinding has been further strengthened in our code by also introducing a non-consistent streamline upwind term. It is noted that, for additional stability of the numerical scheme, Rajagopalan *et al.*[24] have suggested separation of the elastic and viscous stresses (EVSS method). Debae *et al.*[25] also confirmed that such a split of elastic and viscous stresses imparts additional stability to the numerical simulation of viscoelastic flows. Although this approach has not been incorporated into the present numerics, it is possible that such a formulation of the governing equations could further enhance the stability of the present numerical scheme. This possibility should be investigated in future work.

2. GOVERNING EQUATIONS

Assuming a steady, inertia-free, isothermal, incompressible flow with no body force, the conservation equations for momentum and mass are simplified to

$$\nabla \cdot \tilde{\sigma} = 0 \quad \text{in} \quad \Omega, \tag{1}$$

$$\nabla \cdot \hat{u} = 0 \quad \text{in} \quad \Omega, \tag{2}$$

where $\tilde{\sigma}$ is the stress tensor, $\hat{u}$ is the velocity and Ω is the flow domain. For the Leonov model the stress is given by

$$\tilde{\sigma} = -p\tilde{\delta} + 2\eta_\infty \tilde{e} + \tilde{\tau}_e, \tag{3}$$

where p is the pressure, $\tilde{\delta}$ is the unit tensor, η_∞ is the second Newtonian viscosity, $\tilde{e} = \frac{1}{2}(\nabla\hat{u} + \nabla\hat{u}^T)$ and $\tilde{\tau}_e$ is the extra stress tensor due to the viscoelastic nature of the fluid. In the multimode case the extra stress tensor is given by $\tilde{\tau}_e = \sum_{k=1}^{N} \tilde{\tau}_k$, where N denotes the number of modes and $\tilde{\tau}_k$ is the extra stress due to mode k in the viscoelastic constitutive equation.

For planar flow with the Leonov model based upon the rubber elasticity work potential and with strain hardening[2] of the polymer molecules neglected, the extra stress $\tilde{\tau}_k$ is given by

$$\tilde{\tau}_k + \lambda_k \overset{\nabla}{\tilde{\tau}}_k + \frac{1}{2}\frac{\lambda_k}{\eta_k}(\tilde{\tau}_k \cdot \tilde{\tau}_k) = 2\eta_k \tilde{e}, \tag{4}$$

where η_k and λ_k are the viscosity and relaxation time parameters respectively for mode k and the superscript k denotes the upper-convected material derivative defined as

$$\overset{\nabla}{\tilde{\tau}}_k \equiv \frac{D\tilde{\tau}_k}{Dt} - \nabla\hat{u} \cdot \tilde{\tau}_k - \tilde{\tau}_k \cdot \nabla\hat{u}^T, \tag{5}$$

where $D\tilde{\tau}_k/Dt$ is the material derivative of $\tilde{\tau}_k$.

3. CONFIGURATIONAL INCOMPRESSIBILITY

The Leonov model,[2] which was derived from non-equilibrium thermodynamics, has an additional constraint for the Finger tensor, $\tilde{c}_k \equiv \tilde{\delta} + (\lambda_k/\eta_k)\tilde{\tau}_k$. Specifically, $\tilde{c}_k$ in the Leonov model represents the portion of total strain which will be recovered if all the stresses are suddenly released. Since the density of an incompressible viscoelastic medium after unloading must be the same as that before the deformation started, $\rho = \rho_0 = \rho_p$, where ρ, ρ_0 and ρ_p are respectively the density at any instant, the density before the deformation started and the density after unloading. Therefore, besides $\text{trace}(\tilde{e}) = 0$, we must also have $\text{trace}(\tilde{e}_p) = 0$ (where $\tilde{e}_p$ is the non-recoverable portion of $\tilde{e}$), which implies

$$\det \tilde{c}_k = 1, \quad k = 1, \ldots, N. \tag{6}$$

Equation (6), which was considered self-evident by Leonov,[2] was criticized by Giesekus[26] as being unproved from the point of view of the kinematics of randomly distributed polymer molecules. However, Leonov[27] later justified equation (6). It is noted that equations (4) and (6) give four linear equations for three independent components of $\tilde{c}_k$, namely the 11, 22 and 12 ($=21$) components. This appears anomalous at first glance. Furthermore, since we have N kinematic constraints (equation (6)) for the recoverable strain, the constitutive equation (4) should determine the stress due to the recoverable strain only up to N additive constants, which are to be determined as part of the solution to the initial/boundary value problem. This apparent anomaly is resolved by noting that the complete stress due to the recoverable portion of the strain is given in the Leonov model by

$$\tilde{\sigma}_k = -p_k\tilde{\delta} + \tilde{\tau}_k, \quad k = 1, \ldots, N, \tag{7}$$

where $\tilde{\tau}_k$ is governed by equation (4) and the extra pressure p_k is to be determined such that

$$\det\left(\tilde{c}_k - \frac{\lambda_k}{\eta_k} p_k \tilde{\delta}\right) = 1. \tag{8}$$

Since the stress due to the non-recoverable portion of the strain is given by $\tilde{\sigma}_p = -p\tilde{\delta} + 2\eta_\infty \tilde{e}$, where the pressure p is determined from the incompressibility condition (equation (2)), then the total stress is given by

$$\tilde{\sigma} = -p\tilde{\delta} + 2\eta_\infty \tilde{e} + \sum_{k=1}^{N} (\tilde{\tau}_k - p_k \tilde{\delta}). \tag{9}$$

As shown in the Appendix, for the Leonov constitutive equation (4), if the velocity field is divergence-free and $\det(\tilde{c}_k)$ is unity at the entrance, then it will remain unity throughout the flow domain, implying that $p_k = 0$, $k = 1, \ldots, N$, and we are left with only one undetermined constant p to be determined from equation (2). Nevertheless, in a numerical simulation using the finite element method, the divergence-free condition on the velocity field (equation (2)) is satisfied only in a variational sense and not at every point in the flow domain. In any simulation the incompressibility condition can be particularly violated near singularities such as the entrant corner in an entrance flow. Furthermore, even if $\det(\tilde{c}_k) = 1$ at the entrance nodes, owing to the polynomial interpolation of $\tilde{c}_k$, $\det(\tilde{c}_k)$ will not be unity on the portion of the entrance boundary between the nodes. Therefore, in a numerical simulation, $p_k \neq 0$. In the present work, once $\tilde{\tau}_k$ $(k = 1, \ldots, N)$ has been determined (equation (4)), equation (8) is used to determine p_k for each of the N modes. A linear discontinuous interpolation (same as the interpolation for the extra stress tensor) has been used for the extra pressure p_k.

4. NUMERICAL SCHEME

In order to obtain a variational form of the viscoelastic flow problem, we need to define the solution space for the velocity, pressure and extra stress tensor. On the flow domain Ω the space of square-integrable functions is denoted by

$$L^2(\Omega) = \left[u \middle| \int_\Omega |u(x)|^2 \mathrm{d}x < \infty \right] \tag{10}$$

and the Sobolov space as

$$H^1(\Omega) = [u | u \in L^2(\Omega), \quad \nabla u \in (L^2(\Omega))^2] \tag{11}$$

such that the solution space for the velocity is given by

$$V = [\hat{v} | v_i \in H^1, \quad i = 1 \text{ or } 2, \quad v_i = \bar{u}_i \text{ on } \Gamma_u], \tag{12}$$

where v_i is a component of the vector $\hat{v}$ and Γ_u is the part of the boundary Γ where the velocity $\bar{u}_i$ is given. The solution spaces for the pressure (Q), extra stress tensor (W) and extra pressure (S) are then given by

$$Q = L^2(\Omega), \tag{13}$$

$$W = [\tilde{\phi} | \phi_{ij} \in L^2(\Omega), \quad i,j = 1 \text{ or } 2, \quad \phi_{12} = \phi_{21}], \tag{14}$$

$$S = L^2(\Omega), \tag{15}$$

where ϕ_{ij} is a component of $\tilde{\phi}$.

The variational form of the viscoelastic flow problem is: find $(\hat{u}, p, \tilde{\tau}, p_k) \in V \times Q \times W \times S$ such that

$$\langle(\tilde{\sigma}_e + 2\eta_\infty \tilde{e}(\hat{u})) : \tilde{e}(\hat{v})\rangle - \langle p\nabla \cdot \hat{v}\rangle = \langle \hat{T} \cdot \hat{v}\rangle_s, \quad \forall \hat{v} \in V_0, \tag{16}$$

$$\langle q\nabla \cdot \hat{u}\rangle = 0, \quad \forall q \in Q, \tag{17}$$

$$\langle \tilde{\tau}_k : \tilde{\phi}\rangle + \lambda_k[\langle(\hat{u} \cdot \nabla\tilde{\tau}_k) : \tilde{\phi}\rangle - \langle(\nabla\hat{u} \cdot \tilde{\tau}_k) : \tilde{\phi}\rangle - \langle(\tilde{\tau}_k \cdot \nabla\hat{u}^T) : \tilde{\phi}\rangle] + \frac{1}{2}\frac{\lambda_k}{\eta_k}\langle(\tilde{\tau}_k \cdot \tilde{\tau}_k) : \tilde{\phi}\rangle - 2\eta_k\langle\tilde{e}(\hat{u}) : \tilde{\phi}\rangle = 0,$$

$$\forall \tilde{\phi} \in W, \quad k = 1, \ldots, N, \tag{18}$$

$$\left\langle \left[\det\left(\frac{\lambda_k}{\eta_k}(\tilde{\tau}_k - p_k\tilde{\delta}) + \tilde{\delta}\right) - 1 \right]\psi \right\rangle = 0, \quad \forall \psi \in S, \quad k = 1, \ldots, N, \tag{19}$$

where $\langle \cdot \rangle$ and $\langle \cdot \rangle_s$ denote integration over Ω and Γ respectively and $a \cdot b$ and $a : b$ represent scalar and tensor products respectively, with V_0 defined by $\{\hat{v} | v_i \in H^1, \ i = 1 \text{ or } 2, \ v_i = 0 \text{ on } \Gamma_u\}$, $\tilde{\sigma}_e = \sum_{k=1}^{N} \tilde{\sigma}_k$ and $\hat{T}$ denoting the traction on the boundary.

For stability of the numerical scheme, the convection term in equation (18) requires upwind discretization. As mentioned earlier, the method of Lesaint and Raviart[20] has been used in this work to incorporate upwinding; this involves integrating the convection term by parts twice. In the first of the resulting two surface integrals, Fortin and Fortin[18] used the following scheme for the stress values on the sides of the finite elements:

$$\tilde{\tau}_k = \tilde{\tau}_k^e \quad \text{on} \quad \partial m^-, \qquad \tilde{\tau}_k = \tilde{\tau}_k^i \quad \text{on} \quad \partial m^+, \tag{20}$$

where m is the current element, ∂m^- and ∂m^+ are the portions of the finite element boundary where fluid is entering and leaving respectively and $\tilde{\tau}_k^e$ and $\tilde{\tau}_k^i$ are the values of the extra stress tensor on the outer and inner sides of the edge with respect to the current finite element. While determining the second surface integral, $\tilde{\tau}_k = \tilde{\tau}_k^i$ is used everywhere on the element boundary. The method gives the following additional term in the variational form of the constitutive equation (18):

$$\int_{\partial m^-} ((\hat{u} \cdot \hat{n})[\tilde{\tau}_k] : \tilde{\phi}) ds, \tag{21}$$

where $[\tilde{\tau}_k] = \tilde{\tau}_k^e - \tilde{\tau}_k^i$ on the finite element boundary ∂m and $\hat{n}$ is the outward normal to the finite element boundary.

In our work we started with the Lesaint–Raviart method as described above. However, we found that the numerical stability of the scheme is further enhanced if modified as described below. Specifically, instead of using equation (20) in the first of the two surface integrals obtained from integration by parts, we use the following equation for the stress on the boundary of a finite element:

$$\tilde{\tau} = \frac{\tilde{\tau}_k^i - \tilde{\tau}_k^e}{2}\beta + \frac{\tilde{\tau}_k^i + \tilde{\tau}_k^e}{2}, \tag{22}$$

where

$$\beta = \frac{\hat{u} \cdot \hat{n}}{\sqrt{(\hat{u} \cdot \hat{u})}} \quad \text{if} \quad \|\hat{u}\| > 0, \qquad \beta = 1 \quad \text{if} \quad \|\hat{u}\| = 0. \tag{23}$$

With the use of (22), the surface integral term in (21) is modified to

$$\int_{\partial m} (\alpha(\hat{u} \cdot \hat{n})[\tilde{\tau}_k] : \tilde{\phi}) ds, \tag{24}$$

where $\alpha = \frac{1}{2}(1 - \beta)$. It is noted that the surface integral in (24) is performed on the complete element boundary, in contrast with (21) where the integral is performed only on the inflow portion of the boundary of the element. At the entrance of the flow domain, $\tilde{\tau}$ is specified owing to the hyperbolic nature of the constitutive equation such that the surface integral term can be easily determined at the entrance. At the exit of the flow domain the surface integral in (24) vanishes if the flow is normal to the boundary (such that $\beta = 1$). The surface integral also vanishes at solid boundaries (since $\hat{u} = 0$) and where the flow is parallel to the boundary (e.g. along the axis of a symmetric flow domain, since $\hat{u} \cdot \hat{n} = 0$).

As mentioned in Section 1, upwinding in the current numerical scheme has been further strengthened by introducing a non-consistent streamline upwind term in the variational form of the constitutive equation (18) in order to modify the weighting function of the convection term. The additional term is given by

$$\lambda_k \left\langle (\hat{u} \cdot \nabla \tilde{\tau}_k) : \left(\frac{\kappa}{\hat{u} \cdot \hat{u}} \hat{u} \cdot \nabla \tilde{\phi} \right) \right\rangle, \tag{25}$$

where κ is an upwind parameter. It is noted that, in contrast with the non-consistent upwind scheme used here (in which the weighting function is modified for the convection term only), the weighting function in the SUPG method is modified for the complete constitutive equation. The modification of the weighting function in the SUPG method is equivalent to the addition of an artificial diffusion term, with the upwind parameter being equivalent to an artificial diffusivity. For the one-dimensional case, by adding an appropriate amount of artificial diffusion such that the nodal values of the approximate solution are exact. Brooks and Hughes[15] derived a value of $\kappa = |u|h/2$, where h is the uniform mesh size. As discussed by Brooks and Hughes, to avoid crosswind diffusion in the 2D case, the artificial diffusion should not be isotropic, such that the diffusivity should be a tensor. For the rectangular finite element shown in Figure 1, if the velocity is along axis 1, then it is obvious that the artificial diffusivity is

$$\tilde{\kappa} = \frac{uh_1}{2} \begin{bmatrix} 1 & 0 \\ 0 & 0 \end{bmatrix},$$

whereas

$$\tilde{\kappa} = \frac{vh_2}{2} \begin{bmatrix} 0 & 0 \\ 0 & 1 \end{bmatrix}$$

if the velocity is along axis 2. If the velocity is along any other direction, the general form of the artificial diffusivity tensor is $\tilde{\kappa} = \kappa(\hat{i}_u \otimes \hat{i}_u)$, where $\hat{i}_u$ is the unit vector in the direction of the velocity, $\otimes$ denotes the dyadic product of two vectors and κ is the same as the upwind parameter in (25). However, the appropriate value of κ in this general case is not obvious. In particular, Marchal and Crochet[14] and Brooks and Hughes[15] employed *ad hoc* generalizations of the one-dimensional analysis. For the quadrilateral finite elements used by Marchal and Crochet[14] and Brooks and Hughes,[15] κ was defined in terms of the velocity at the centroid and the principal vectors of the finite element. Two different values were suggested by Brooks and Hughes,[15] namely

$$\kappa = \tfrac{1}{2}(|u_\eta| + |u_\zeta|), \qquad \kappa = \tfrac{1}{2}\sqrt{(u_\eta^2 + u_\zeta^2)}, \tag{26}$$

where $n_\eta = \hat{u}_0 \cdot \hat{h}_\eta$ and $u_\zeta = \hat{u}_0 \cdot \hat{h}_\zeta$, in which $\hat{u}_0$ is the velocity at the centroid of the finite element and $\hat{h}_\eta$ and $\hat{h}_\zeta$ are the vectors along the two principal directions of the quadrilateral finite element, with magnitude equal to the size of the element along each respective direction. The latter of the two values for κ in equation (26) was used by Marchal and Crochet.[14] As noted by Rao and Finlayson,[28]

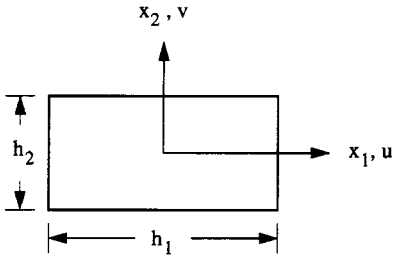

Figure 1. Co-ordinate system, velocity components and finite element dimensions for defining artificial diffusivity in SUPG method

generalization of (26) to triangular elements is not obvious. In an attempt to approximate (26), Rao and Finlayson used two different expressions for κ. One of these two suggested expressions has been used by Chang and Yang[29] even for quadrilateral elements.

In this work, in the local co-ordinate system (x', y'), with x' aligned along the velocity at every point inside a finite element (Figure 2), we have used the artificial diffusivity

$$\tilde{\kappa} = \frac{\|\hat{u}\|h}{2}\begin{bmatrix} 1 & 0 \\ 0 & 0 \end{bmatrix},$$

where h is as shown in Figure 2, for both a quadrilateral as well as a triangular element. In the global co-ordinate system (X, Y), the diffusivity is

$$\tilde{\kappa} = \frac{\|\hat{u}\|h}{2}(\hat{i}_u \otimes \hat{i}_u).$$

Therefore, in (25), $\kappa = \|\hat{u}\|h/2$, with h as defined in Figure 2. It is noted that, in contrast with the approach followed in the literature,[14–16,28,29] in the current work h is not a constant for a given finite element, such that, while performing the integration in (25), an appropriate value for κ is determined by the scheme described above at each quadrature point.

5. ITERATION SCHEME

Owing to the non-linear nature of the viscoelastic constitutive equation (4), it is solved iteratively. Two iteration schemes have typically been used in the literature. In the simpler approach the constitutive equation is linearized by using the Newton–Raphson method and the complete set of

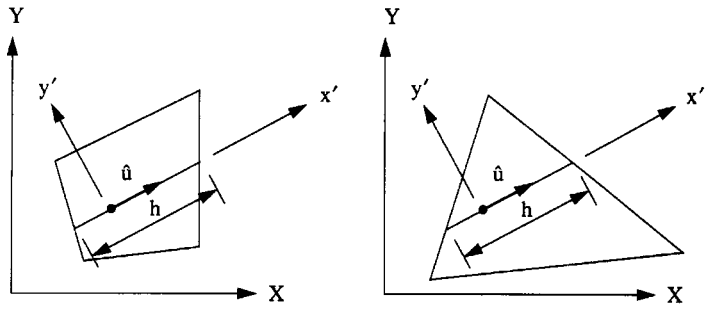

Figure 2. Local and global co-ordinate systems for defining artificial diffusivity for (a) quadrilateral and (b) triangular finite elements

equations (16)–(19) is solved simultaneously. Owing to its superior convergence rate, such a scheme has been used extensively in the literature, e.g. by Marchal and Crochet[14] and Rao and Finlayson.[28] However, simultaneous solution of the velocity, pressure and stress equations, which can easily be of the order of 10 000 equations, even with only one mode in the constitutive equation, makes the scheme computationally inefficient. Furthermore, owing to the non-linear nature of the constitutive equation, the matrix as well as the forcing vector for the simultaneous linear equations needs to be updated in every iteration. We started using this scheme in the present work but found it to be impractical when more than one mode is used in the constitutive equation.

In contrast, the Picard iteration scheme[3,5,6,18,19,21] solves the problem in two stages. Starting with an initial approximation to the velocity and stress fields, in the first step the momentum and mass conservation equations are solved, treating the extra stress from the viscoelastic constitutive equation as a known body force. With known velocity field, the constitutive equation is then solved to update the extra stress tensor. The two steps are then repeated successively until convergence. Besides breaking the problem into two parts, this scheme is especially desirable for the viscoelastic flow problem for two reasons. First of all, since the momentum and mass conservation equations are linear, the matrix for the system of linear equations for the Stokes flow problem is formed and triangulated using LU decomposition only in the first iteration. In subsequent iterations, as the extra stress changes, only the forcing vector on the right-hand side of the linear equations changes, such that the solution requires only back substitution. Secondly, in the case of multiple modes in the constitutive equation, the equations for each mode are decoupled and can be solved separately in the Picard scheme. However, as noted by many researchers in the literature,[3,5,6,18,19,21] such a scheme tends to have poor convergence characteristics. In order to stabilize the iteration scheme, Upadhyay and Isayev[3] added an extra term $\eta_a(\tilde{e}^m - \tilde{e}^{m-1})$ to the momentum equation, where $\tilde{e}^m$ and $\tilde{e}^{m-1}$ are the strain rate tensors based upon the velocity field in the current and previous iterations respectively and η_a can be viewed as an artificial viscosity. In all the simulations presented in Section 8, we have followed Upadhyay and Isayev, taking $\eta_a = \sum_{k=1}^{N} \eta_k$, where η_k is the same as in (4). Furthermore, 30 per cent underrelaxation has been used in successive iterations for velocity as well as the extra stress tensor.

With known velocity field, the only non-linear term in the constitutive equation, $\frac{1}{2}(\lambda_k/\eta_k)(\tilde{\tau}_k \cdot \tilde{\tau}_k)$, has been linearized by using the Newton–Raphson method. Even though a discontinuous discretization has been used for the stress tensor, the equations for the stress variables on each finite element are coupled with the equations for the stress variables on the neighbouring elements through the boundary integral term (24) arising from the GLR method. In the present work the constitutive equation has been solved at the element level, all the elements being scanned repeatedly until convergence (Figure 3). In the multimode case the number of required iterations for the inner loop in Figure 3 has been found to increase with relaxation time, being greatest for the mode with the largest relaxation time.

If $u_m = \sqrt{(u_i u_i)}$ and $\tau_m = \sqrt{(\tau_{ij}\tau_{ij})}$ $(i, j = 1 \text{ or } 2)$ are used to define the magnitude of velocity and stress at a point, then we have used the following criteria to define convergence:

$$\frac{\|p^n - p^{n-1}\|}{\|p^n\|}, \frac{\|u_m^n - u_m^{n-1}\|}{\|u_m^n\|}, \frac{\|\tau_m^n - \tau_m^{n-1}\|}{\|\tau_m^n\|} \leqslant (1 - r_f)\varepsilon_r,$$

where $\|\cdot\|$ denotes the L^2 norm, r_f $(= 0{\cdot}3)$ is the underrelaxation factor, where $r_f = 0$ corresponds to straight relaxation, ε_r is the maximum error allowed and n denotes the iteration number for the outer loop in Figure 3. In the present work we started with $\varepsilon_r = 10^{-2}$ but the results obtained were found to be not fully converged. A maximum error of $\varepsilon_r = 10^{-3}$ was found to be sufficiently refined to give the converged results reported below. By using the Picard iteration scheme with the element-level

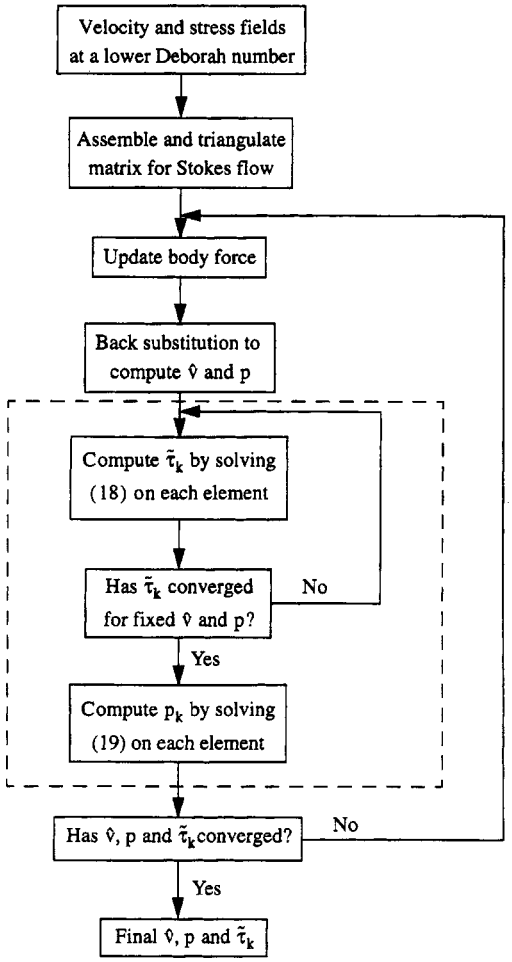

Figure 3. Flow diagram of algorithm used to solve viscoelastic flow equations by using Picard iteration scheme and solving constitutive equation at element level. The steps inside broken rectangle are executed separately for each mode in the constitutive equation

solution of the constitutive equation, the calculations for velocity, pressure, extra stress tensor and extra pressure could be performed easily on the IRIS-INDIGO work station from Silicon Graphics, Inc.

6. LEONOV MODEL PARAMETERS

Two different materials have been used in this work to simulate flow in a 4 : 1 abrupt planar contraction. For PTT rubber at 100 °C we used the three-mode Leonov model as given by Isayev and Huang[4]:

$$\eta_\infty = 6{\cdot}4 \text{ Pa s},$$
$$\eta_k = 1{\cdot}3 \times 10^5,\ 1{\cdot}54 \times 10^4,\ 3{\cdot}11 \times 10^2 \text{ Pa s},$$
$$\lambda_k = 6{\cdot}3,\ 0{\cdot}109,\ 0{\cdot}0013 \text{ s}.$$

It should be noted that Isayev and Huang used an extended Leonov model which includes a yield stress. However, they found that the yield stress has only a minor influence on the predicted entrance loss and the influence diminishes as the flow rate is increased. The entrance flow has also been simulated for polystyrene with two different Leonov model fits. For polystyrene (PS) the parameters used in the simulation based upon the Leonov model are as follows (at 210 °C):

(a) two-mode fit

$$\eta_\infty = 26{\cdot}73 \text{ Pa s},$$
$$\eta_k = 1{\cdot}369 \times 10^3,\ 3{\cdot}219 \times 10^2 \text{ Pa s},$$
$$\lambda_k = 1{\cdot}095 \times 10^{-1},\ 6{\cdot}939 \times 10^{-3} \text{ s};$$

(b) three-mode fit

$$\eta_\infty = 4{\cdot}605 \text{ Pa s},$$
$$\eta_k = 1{\cdot}298 \times 10^3,\ 4{\cdot}167 \times 10^2,\ 4{\cdot}449 \times 10 \text{ Pa s},$$
$$\lambda_k = 1{\cdot}354 \times 10^{-1},\ 1{\cdot}135 \times 10^{-2},\ 5{\cdot}393 \times 10^{-4} \text{ s}.$$

These values have been obtained by fitting steady shear viscosity data for a commercial-grade PS (Styron 615/Dow), using a simplex method[30] to obtain the best fit. The resulting fits with the experimental results for polystyrene are shown in Figure 4, which also shows a similar plot for the PTT rubber by Isayev and Huang.[4] It is noted that the predicted viscosity from the two-mode Leonov model starts to deviate from experimental results at a shear rate $\dot{\gamma}$ of about $2{\cdot}5 \times 10^3$ s^{-1}, corresponding to a fully developed downstream wall shear stress of about $1{\cdot}25 \times 10^5$ Pa for the PS material at 210 °C. On the other hand, the predictions from the three-mode model are valid up to a shear rate of 2×10^4 s^{-1}, corresponding to a wall shear stress of about 2×10^5 Pa. Using the Leonov model parameters given above, the predicted variation in the primary normal stress coefficient $\psi_1 \equiv N_1/\dot{\gamma}^2$, with N_1 being the first normal stress difference, is shown in Figure 5.

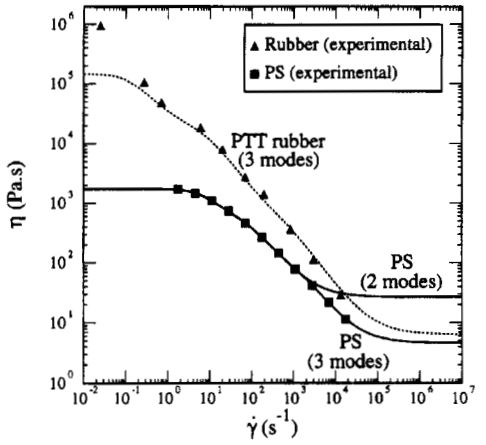

Figure 4. Experimental and Leonov model fits for viscosity of rubber and polystyrene

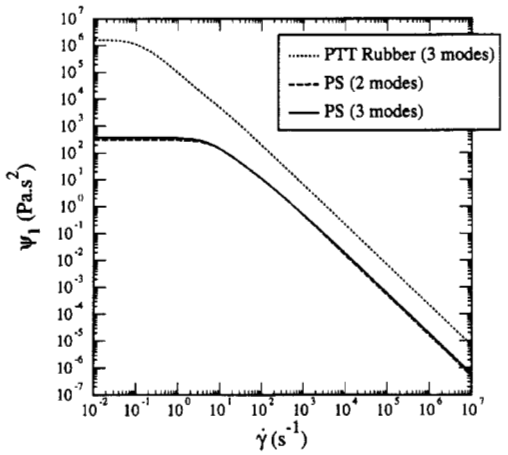

Figure 5. Primary normal stress coefficient for rubber and polystyrene based upon Leonov model fits of steady shear viscosity

7. POISEUILLE FLOW

To verify the accuracy of the numerical scheme presented in Sections 4 and 5, the three-mode Leonov model parameters for polystyrene given in the last section were used to simulate a pressure-driven flow in a planar channel. To characterize the flow, a non-dimensional shear rate (Deborah number *De*) has been defined as

$$De = \frac{3U}{b}\lambda_0, \tag{27}$$

where U is the mean velocity in the channel, b is the half-gap height of the channel and λ_0 is the characteristic relaxation time of the fluid at low shear rates, namely[3]

$$\lambda_0 = \frac{\sum_{k=1}^{N} \eta_k \lambda_k}{\eta_\infty + \sum_{k=1}^{N} \eta_k}. \tag{28}$$

The zero-shear-rate relaxation time defined above is a convenient parameter for comparing the characteristic time of various polymers. However, it should be noted that the actual relaxation time decreases significantly at higher shear rate, a characteristic arising from the non-linearity of the Leonov model. The Weissenberg number *We*, which is an alternative measure of the elasticity of the flow, is defined as

$$We = \frac{N_1}{2\tau_{12}}, \tag{29}$$

where τ_{12} is the shear stress in simple shear flow. The variation in *We* as a function of shear stress in simple shear flow is shown in Figure 6 and tabulated in Table I. It is noted that *We* increases with shear stress in the valid range of data for the two- and three-mode Leonov models, attaining its maximum value in the vicinity of the respective limits of the fits for PS in Figure 4 and then decreasing monotonically. The maximum values of *We* for the two- and three-mode fits of polystyrene are 3·2 and 6·1 respectively. The Weissenberg number also increases for the rubber compound over the range of experimental data presented by Isayev and Huang.[4] Even though the

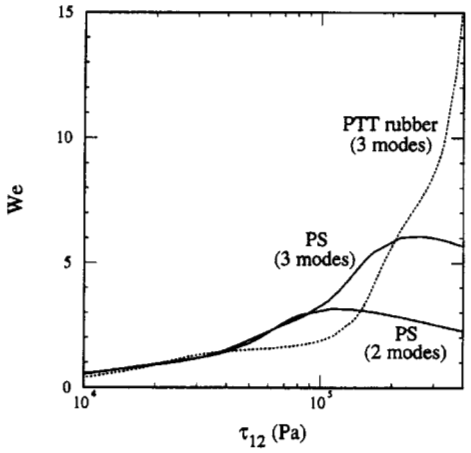

Figure 6. Weissenberg number versus shear stress in simple shear flow using multimode Leonov model for rubber and polystyrene

curve in Figure 6 for the rubber compound is shown only in the range in which the experimental results were given,[4] the curve for the rubber compound attains a maximum at a stress level beyond the range of shear stress in Figure 6 (namely a value of about 33·4 at a shear stress of $7{\cdot}8 \times 10^5$ Pa) and then decreases sharply as the shear stress increases further.

Three successively refined finite element meshes shown in Figure 7 have been used to check the convergence of the numerical predictions. Using the symmetry of the problem, only the flow on one side of the axis of symmetry has been simulated. Besides the symmetry condition along the axis and the no- slip condition on the solid walls, the velocity and stresses for fully developed channel flow[31] have been specified at the entrance, whereas fully developed channel flow has been imposed on the velocity alone at the exit. For the three-mode Leonov model for polystyrene at $De = 100$ the predicted

Table I. Strain rate, shear stress and Weissenberg number versus Deborah number for simple shear flow in case of (a) PTT rubber at 100 °C and (b, c) polystyrene at 210 °C

				(a) PTT rubber			
De	10	20	50	100	200	500	670
$\dot{\gamma}$ (s^{-1})	2·2	4·4	13·1	35·2	83·5	194·7	249·0
τ (10^5 Pa)	0·54	0·79	1·25	1·56	1·81	2·17	2·32
We	1·53	1·67	2·30	3·43	4·81	6·29	6·71
				(b) Polystyrene with two-mode Leonov model			
De	10	20	50	100	200	500	670
$\dot{\gamma}$ (s^{-1})	160·5	371·8	955·6	1729	3045	6607	7759
τ (10^5 Pa)	0·46	0·61	0·81	1·03	1·39	2·35	2·66
We	1·63	2·21	2·88	3·12	3·11	2·74	2·63
				(c) Polystyrene with three-mode Leonov model			
De	10	20	50	100	200	300	453
$\dot{\gamma}$ (s^{-1})	143·0	313·2	777·0	1574	3443	5400	8181
τ (10^5 Pa)	0·43	0·56	0·78	1·00	1·25	1·40	1·57
We	1·63	2·12	2·69	3·22	4·06	4·64	5·18

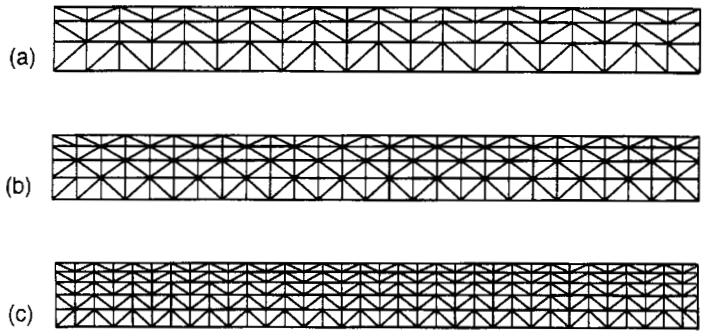

Figure 7. Successively refined finite element meshes used for simulating planar flow in a channel: (a) mesh A; (b) mesh B; (c) mesh C. The upper boundary corresponds to the solid wall and the lower boundary to the axis of symmetry

velocity profiles across the planar channel obtained by using the numerical scheme described in Sections 4 and 5 are shown in Figure 8. For all three finite element meshes in Figure 7 the predicted velocity profile agrees well with the theoretical velocity profile. The numerical predictions obtained by using the SU scheme in conjunction with the GLR method are in excellent agreement with those obtained by using the GLR method alone. In addition, the predicted pressure gradient also agrees well with the theoretical value, with less than 1 per cent error for all three meshes. Figures 9(a) and 9(b) show the first normal stress difference and the extra shear stress respectively across the channel. The predicted stresses agree well with the theoretical values for the three-mode Leonov model. Even for the extra stress tensor, addition of the SU term (equation (25)) has no significant effect on the accuracy of the predictions. However, as will be seen in the next section, the SU term significantly improves the stability of the numerical scheme.

8. FOUR-TO-ONE ENTRANCE FLOW

The numerical scheme presented in Sections 4 and 5 has also been applied to a planar 4 : 1 abrupt contraction, which has been extensively used as a benchmark test in the literature. The dimensions of the flow domain and the three successively refined finite element meshes used are shown in Figures

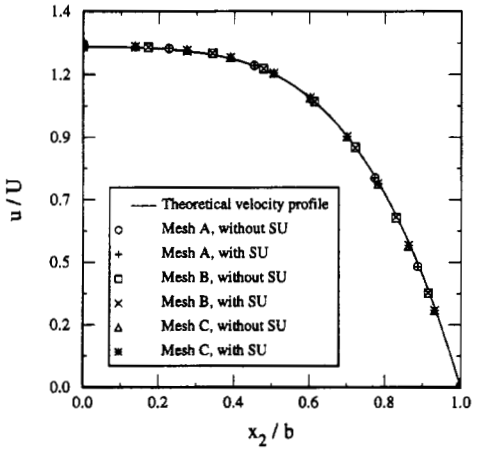

Figure 8. Velocity distribution across planar channel for three-mode Leonov model for polystyrene at $De = 100$. Finite element meshes A, B and C are shown in Figure 7. Results are essentially invariant in the x_1-direction

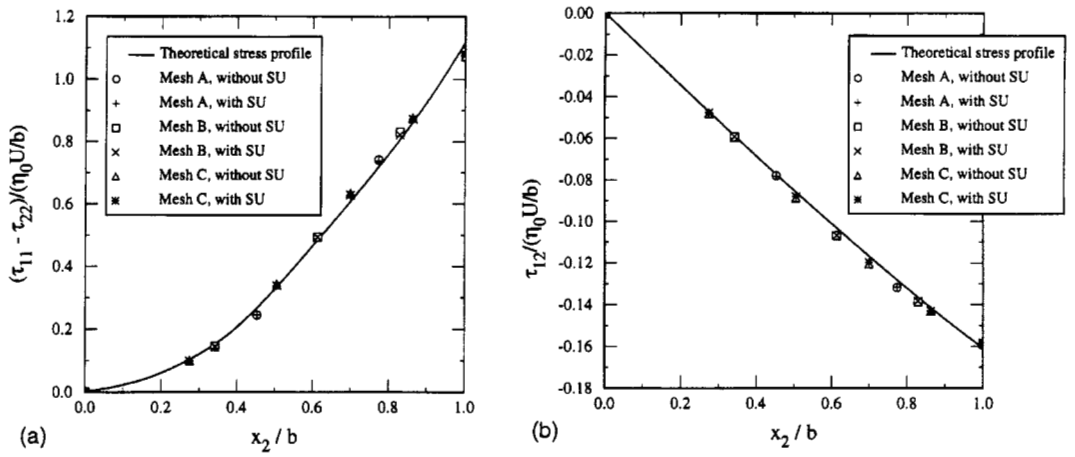

Figure 9. (a) First normal stress difference and (b) extra shear stress across channel for three-mode Leonov model for polystyrene at $De = 100$. The zero-shear-rate viscosity is $\eta_0 = \eta_\infty + \sum_{k=1}^{N} \eta_k$

10 and 11 respectively. Besides the symmetry condition along the axis and the no-slip condition on the solid walls, the velocity and stresses for fully developed channel flow have been specified at the entrance, whereas fully developed channel flow has been imposed on the velocity alone at the exit. To define the Deborah number for a 4 : 1 entrance flow, the mean velocity and the half-gap height of the downstream channel have been used in equation (27).

A quantity of prime interest in this study is the extra pressure drop (i.e. entrance loss) due to the abrupt contraction. It is noted that for fully developed channel flow of the Leonov model, $p^* \equiv p - \tau_{22}$ (and not p) is constant across a cross-section, where 1 denotes the flow direction and 2 the transverse direction. A flush-mounted pressure transducer on the wall will measure p^*. In order to be able to compare the predictions with experimental results, the entrance loss is defined in terms of p^* as

$$L_e = \frac{p_e}{\partial p_2} = \frac{\Delta p^* - \Delta p_1 - \Delta p_2}{\partial p_2}, \tag{30}$$

where Δp^* is the total calculated drop in p^* in the entrance flow, p_e is the extra pressure drop in the entrance flow, Δp_1 and Δp_2 are the pressure drop for fully developed flow in the entry and exit channels respectively and ∂p_2 is the magnitude of the fully developed axial pressure gradient in the exit channel.

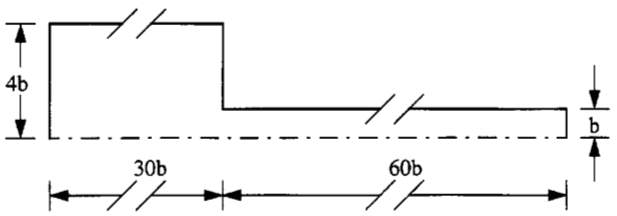

Figure 10. Dimensions of flow domain used for simulating flow with 4 : 1 abrupt planar contraction

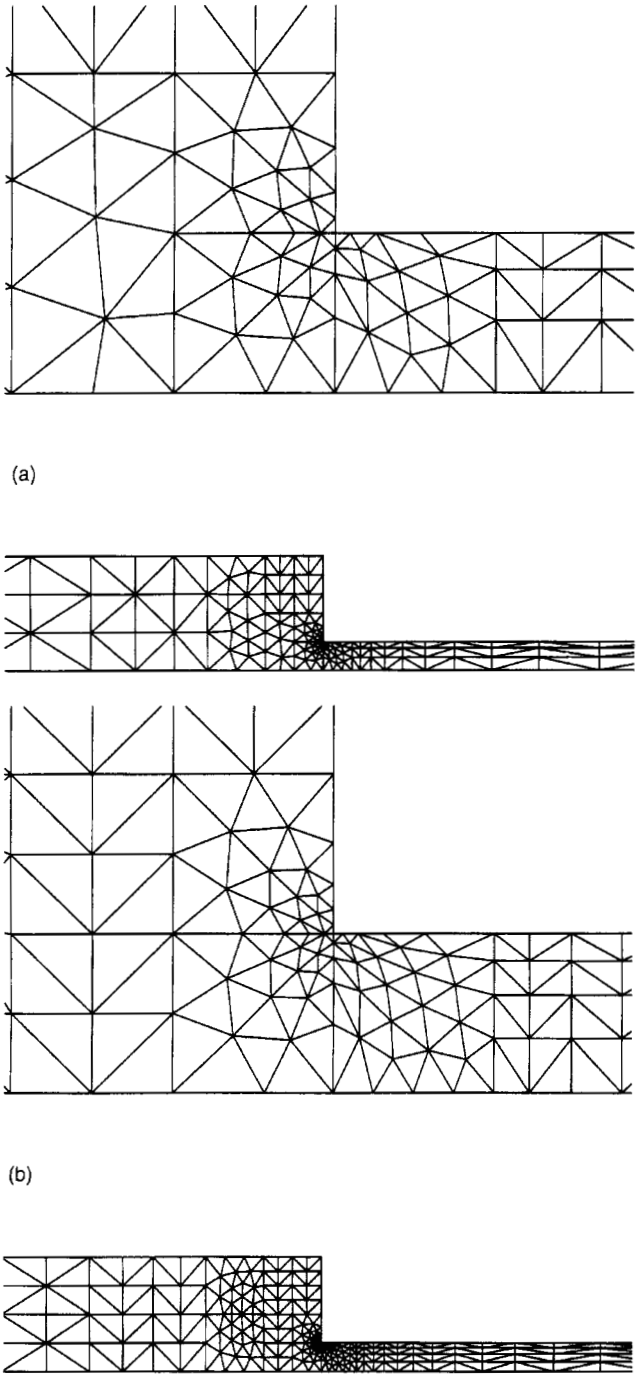

Figure 11. Successively refined finite element meshes ((a) mesh A; (b) mesh B; (c) mesh C) in vicinity of entrant corner (top) and over more extension region (bottom) used for simulating planar flow with 4 : 1 abrupt contraction. The three equal-sized isosceles right triangles adjacent to the entrant corner have their shorter sides equal to 0·094b, 0·057b and 0·039b for meshes A, B and C respectively. Beyond the portion of the flow domain shown in the bottom parts, the finite element length along the flow direction continues to increase in the upstream and downstream sections, becoming 3·8b, 2·9b and 2·2b near the entrance for meshes A, B and C respectively and becoming correspondingly 8·1b, 6·1b and 4·7b near the exit

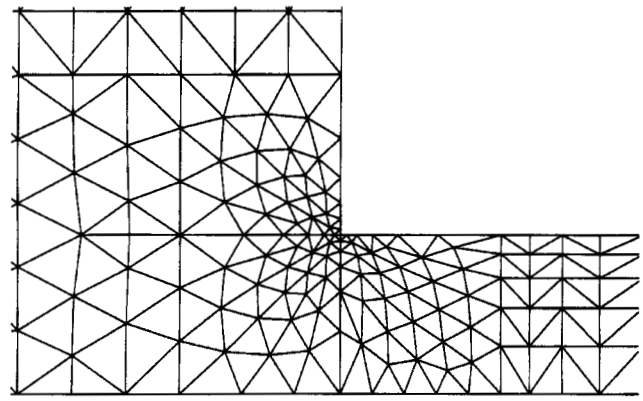

(c)

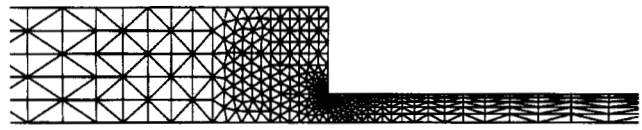

Figure 11. (*continued*)

With the use of the SU scheme in combination with the GLR method, for mesh C the results converged up to $De = 670$ for the rubber compound and up to $De = 600$ and 453 for polystyrene with two and three modes respectively. The simulation started to diverge at much smaller Deborah number if the SU scheme was not used. With the GLR method alone, the results converged up to $De = 92$ for the rubber compound and up to $De = 67$ and 20 for polystyrene with two and three modes respectively.

For the three successively refined meshes in Figure 11, velocity and pressure variations along the centreline for the flow of the rubber compound at $De = 200$ are shown in Figures 12 and 13 respectively. The velocity variation obtained by using the coarse mesh (A) shows slight fluctuations, whereas the two finer meshes (B and C) give smooth velocity variation along the centreline. The excellent agreement between the velocity and pressure distributions obtained by using meshes B and C also confirms convergence with respect to mesh refinement. To examine the effect of the SU scheme on the accuracy of the numerical predictions, Figures 14 and 15 compare the velocity and pressure variations respectively along the centreline for the flow of PTT rubber at $De = 50$. The excellent agreement between the numerical predictions with and without the SU scheme shows that the SU scheme improves the stability of the numerical scheme without any significant adverse effect on the accuracy of the numerical predictions.

Figure 16 shows the centreline velocity for the 4 : 1 entrance flow for the rubber compound and polystyrene at various *De*. As expected, as the flow elasticity is increased, the overshoot in the centreline velocity near the entrance plane increases and a longer distance is required to reach a fully developed flow in the downstream channel. For the maximum *De* reached in this work, the flow was found to become fully developed significantly before the downstream exit $x_1/b = 60$ is reached. For rubber (Figure 16(a)) as well as polystyrene (Figure 16(b)) the asymptotic downstream centreline velocity decreases with increasing flow rate (i.e. *De*), reflecting an increased shear thinning.

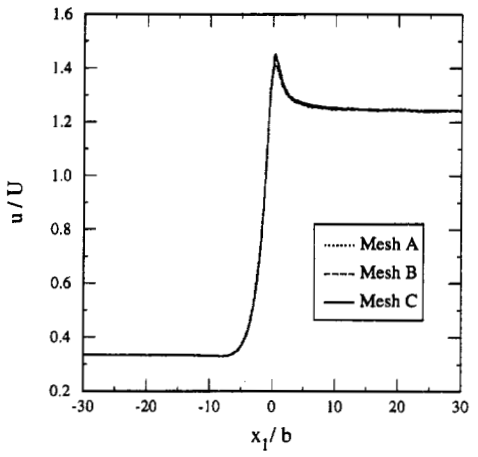

Figure 12. Centreline velocity for 4 : 1 abrupt contraction at $De = 100$ for rubber compound with three-mode Leonov model; $x_1/b = 0$ at abrupt contraction

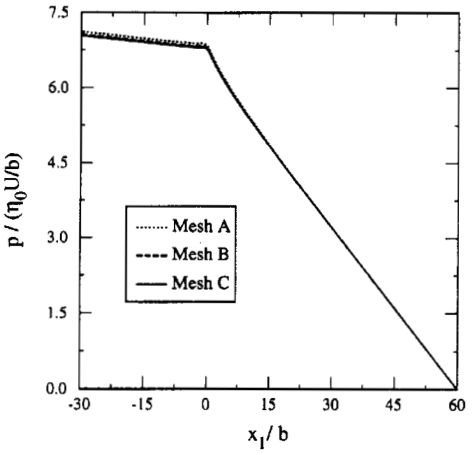

Figure 13. Pressure along centreline of 4 : 1 contraction at $De = 100$ for rubber compound with three-mode Leonov model

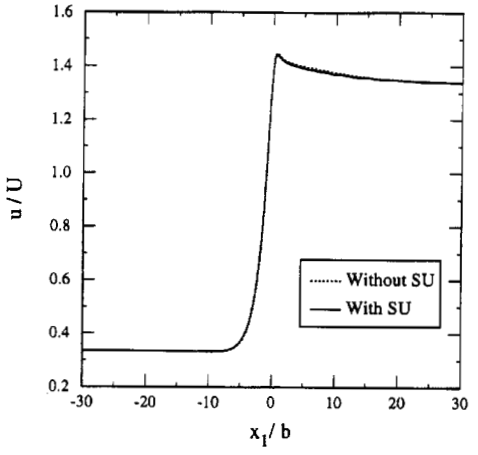

Figure 14. Centreline velocity for 4 : 1 contraction at $De = 50$ for rubber compound with and without streamline upwinding

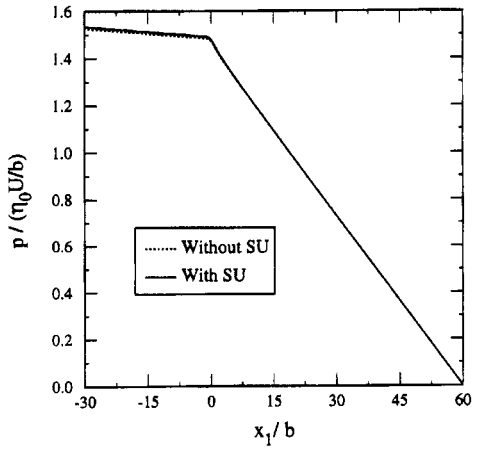

Figure 15. Pressure along centreline of 4 : 1 coontraction at $De = 50$ for rubber compound with and without streamline upwinding

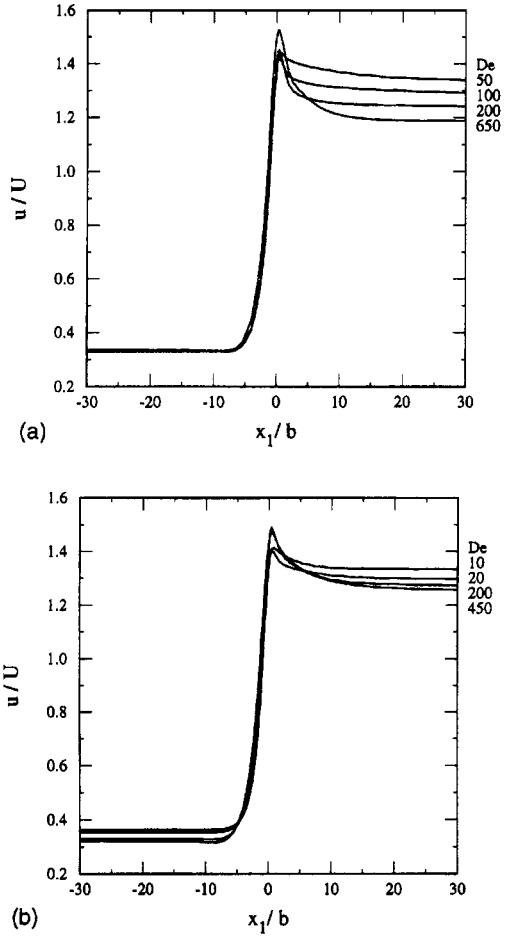

Figure 16. Centreline velocity for 4 : 1 abrupt planar contraction at various Deborah numbers for (a) rubber and (b) polystyrene with three-mode Leonov model; $x_1/b = 0$ at abrupt contraction

To depict the increase in the recirculation zone with flow rate, unit vectors along the direction of velocity at various Deborah numbers are shown in Figures 17 and 18 for the rubber and polystyrene respectively. As expected, the recirculation region grows appreciably with *De*.

For the planar 4 : 1 entrance flow of the rubber compound, the total pressure drop between $x_1/b = -20$ and 20 ($b = 1$ mm) was experimentally measured by Isayev and Huang.[6,32] A comparison between their experimental results and the corresponding numerical predictions from the present work is presented in Figure 19. For the range of flow rate over which the current numerical results converged, the numerical predictions agree well with the experimental values. As a point of reference, Figure 19 also shows the pressure drop based upon the calculated upstream and downstream fully developed pressure gradients multiplied by the respective lengths of each channel section.

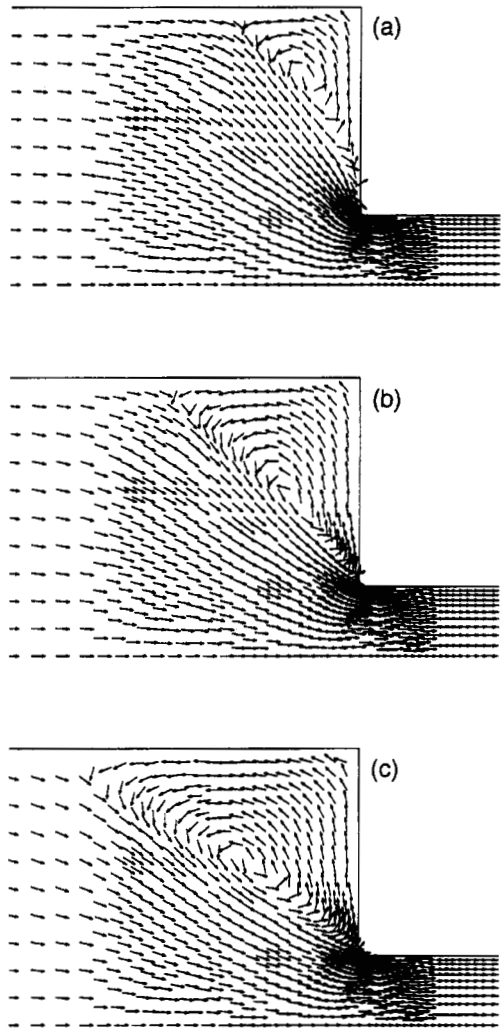

Figure 17. Recirculation in 4 : 1 abrupt planar contraction for PTT rubber compound at *De* = (a) 10, (b) 100 and (c) 650; arrows indicate velocity direction

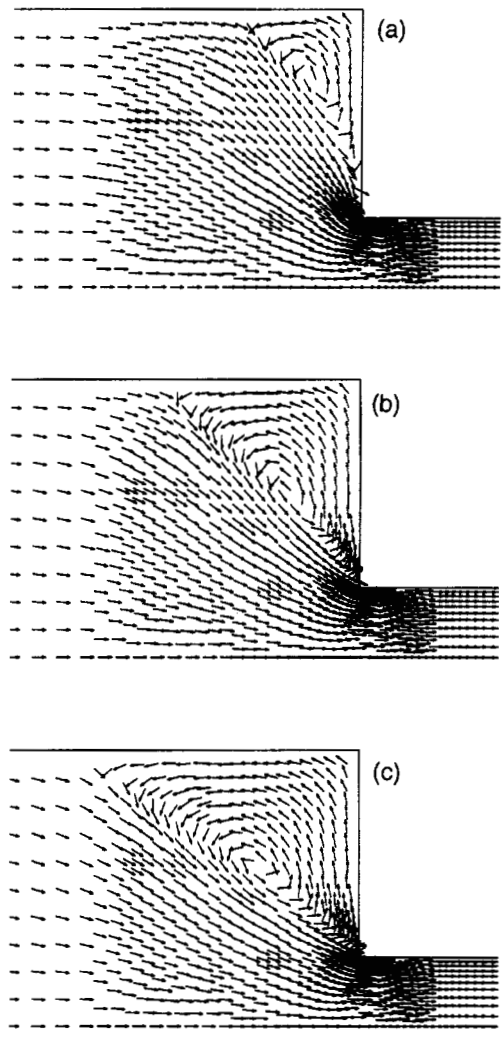

Figure 18. Recirculation in 4 : 1 abrupt planar contraction for polystyrene (three-mode fit) at De = (a) 10, (b) 100 and (c) 450; arrows indicate velocity direction

The predicted extra pressure loss for polystyrene is shown in Figure 20, where comparison is made with an experimental correlation based[33] upon cumulative data in the literature for commercial-grade polystyrenes. Unfortunately, it is seen that the predictions are significantly smaller than the experimental correlation, even allowing a 100 per cent scatter in the underlying cumulative data.[33] It should be noted that the latter data include both axisymmetric (from capillary rheometer) and planar (from slit rheometer) measurements with no systematic difference between the two cases. Further, since each data typically correspond to a contraction ratio much larger than 4 : 1, we have run our simulation also for a 10 : 1 planar contraction. As indicated in Figure 20, the increased contraction ratio does increase the predicted juncture loss, as would be expected, but it still lies significantly below the experimental correlation.

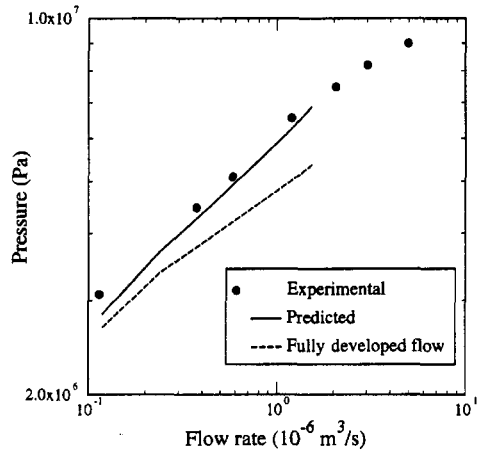

Figure 19. Experimental[6,32] and predicted (present work) total pressure drop between $x_1/b = -20$ and 20 for 4 : 1 abrupt planar entrance flow of rubber compound

As a further check on the predicted results in Figure 20, we have generated a different set of Leonov model constants by fitting dynamic rather than steady shear data. Specifically, we have fitted the dynamic loss and storage modulus data of Pfandl *et al.*[34] for a different commercial-grade PS. However, the resulting predictions for the 4 : 1 planar contraction are essentially unchanged from those presented in Figure 20.

Faced with the significant discrepancy between the simulated and experimental results in Figure 20, we might be led to question the accuracy of the Leonov constitutive equation in the present application. In this regard it might be noted that Larson[35] has indicated that the Leonov model gives

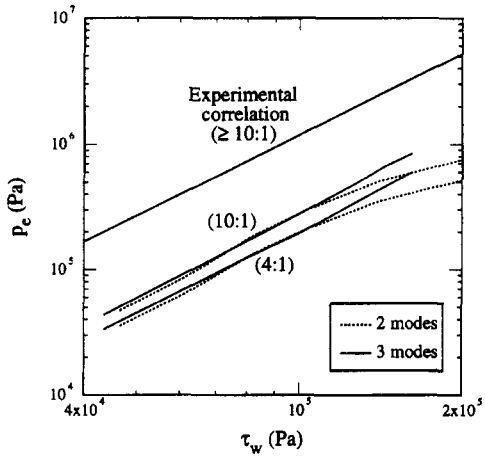

Figure 20. Predicted extra pressure loss for 4 : 1 planar abrupt contraction for polystyrene based on two- and three-mode Leonov models. The experimental correlation[33] corresponds to cumulative data in the literature for commercial-grade polystyrenes, as discussed further in the text

qualitative but not quantitative predictions under elongational flow conditions. On the other hand, Upadhyay and Isayev[3,36,37] have shown by extensive comparisons with experimental data that the Leonov model does have reasonable predictive capabilities under elongational or combined shear/elongational situations. Accordingly, the present discrepancy indicated in Figure 20 remains unexplained and awaits further work in the area.

In closing this section, it should be noted that a marching in Deborah number was required in order to obtain convergence at higher Deborah number. The Deborah number step ranged from 10 to 100. For example, for the three-mode Leonov model for the rubber compound, when the Deborah number for the 4 : 1 abrupt contraction was increased from 100 to 200, 137 iterations were required in the outer loop of Figure 3 with about 32, 11 and 4 iterations required in the inner loop for the first, second and third modes respectively. The complete calculation, including all the iterations in the inner and outer loops, required 55·43 min of computation time on the IRIS-INDIGO with a total number of 866 elements, 1374 vertex nodes and 509 mid-side nodes, corresponding to mesh C in Figure 11.

9. CONCLUSIONS

An efficient algorithm for simulating planar viscoelastic flows has been developed. The excellent efficiency of the algorithm is attributed to an element-level solution of the constitutive equation along with a Picard iteration scheme. The corresponding software, employing the constitutive equation of Leonov, has been used to simulate the flow of two different polymers in channels with abrupt contractions. The numerical simulation converged up to a Weissenberg number of 6·71 for a rubber and up to 5·18 for a commercial-grade polystyrene. The predicted entrance loss is in reasonable agreement with experimental results for the rubber but considerably below those for the polystyrene, indicating a need for further investigation.

ACKNOWLEDGEMENTS

The major portion of this work has been supported by the industrial consortium of the Cornell Injection Molding Program (CIMP). We would like to thank Professor J. T. Jenkins (Theoretical and Applied Mechanics Department, Cornell University) for his helpful discussions. Parts of the calculations were performed on the Cornell National Supercomputer Facility, a resource of the Cornell Theory Center which receives major funding from the National Science Foundation and New York State.

APPENDIX: PROOF OF $\det(c_k) = 1$ CONDITION IN PLANAR LEONOV MODEL

Ignoring the subscript k, the material derivative of the determinant of the Finger tensor for each mode of the Leonov model is given by

$$\frac{\mathrm{D}}{\mathrm{D}t}\det(\tilde{c}) = c_{11}\frac{\mathrm{D}c_{22}}{\mathrm{D}t} + c_{22}\frac{\mathrm{D}c_{11}}{\mathrm{D}t} - 2c_{12}\frac{\mathrm{D}c_{12}}{\mathrm{D}t}. \tag{31}$$

From the constitutive equation (4), material derivatives of the three components of the Finger tensor are

$$\frac{Dc_{11}}{Dt} = 2c_{11}v_{1,1} + 2c_{12}v_{1,2} - \frac{1}{2\lambda}(c_{11}^2 + c_{12}^2 - 1), \tag{32}$$

$$\frac{Dc_{12}}{Dt} = c_{11}v_{2,1} + c_{22}v_{1,2} - \frac{1}{2\lambda}(c_{11} + c_{22})c_{12}, \tag{33}$$

$$\frac{Dc_{22}}{Dt} = 2c_{21}v_{2,1} + 2c_{22}v_{2,2} - \frac{1}{2\lambda}(c_{12}^2 + c_{22}^2 - 1), \tag{34}$$

where $v_{i,j} = \partial v_i/\partial x_j$, $i, j = 1$ or 2. The incompressibility constraint (equation (2)) has also been used to obtain equation (33). Using equations (31)–(34) along with the incompressibility constraint and the condition $\det(c_k) = 1$, it can be easily shown that

$$\frac{D}{Dt}\det(\tilde{c}_k) = 0. \tag{35}$$

Hence, if $\det(c_k) = 1$ at the entrance and the flow field is divergence-free, then $\det(c_k) = 1$ everywhere in the flow domain.

REFERENCES

1. R. G. Larson, *Constitutive Equations for Polymeric Melts and Solutions*, Butterworths, Boston, MA, 1988.
2. A. I. Leonov, 'Non-equilibrium thermodynamics and rheology of viscoelastic polymer media', *Rheol. Acta*, **15**, 85–98 (1976).
3. R. K. Upadhyay and A. I. Isayev, 'Simulation of two-dimensional planar flow of viscoelastic fluid', *Rheol. Acta*, **25**, 80–94 (1986).
4. A. I. Isayev and Y. H. Huang, 'Unsteady flow of rubber compounds at injection molding conditions', *Adv. Polym. Technol.*, **9**, 167– 180 (1989).
5. M. A. Hulsen and J. V. D. Zanden, 'Numerical simulation of contraction flows using a multimode Giesekus model', *J. Non-Newtonian Fluid Mech.*, **38**, 183–221 (1991).
6. A. I. Isayev and Y. H. Huang, 'Planar contraction or expansion flow of a viscoelastic plastic medium: experimentation and simulation', in D. A. Siginer (ed.), *Recent Advances in Non-Newtonian Flows*, AMD Vol. 153, FED Vol. 141, ASME, New York, 1992, pp. 113–128.
7. R. Keunings, in C. L. Tucker (ed.), *Fundamentals of Computer Modelling for Polymer Processing*, Hanser, Munich, 1989, Chap. 9.
8. D. D. Joseph, M. Renardy and J. C. Saut, 'Hyperbolicity and change of type in the flow of viscoelastic fluids', *Arch. Rat. Mech. Anal.*, **87**, 213–251 (1985).
9. F. Dupret and J. M. Marchal, 'Loss of evolution in the flow of viscoelastic fluids', *J. Non-Newtonian Fluid Mech.*, **20**, 143–171 (1986).
10. A. I. Leonov, 'Analysis of simple constitutive equations for viscoelastic liquids', *J. Non-Newtonian Fluid Mech.*, **42**, 323–350 (1992).
11. I. Babuska, 'Error-bounds for finite element method', *Numer. Math.*, **16**, 322–333 (1971).
12. F. Brezzi, 'On the existence, uniqueness and approximation of saddle-point problems arising from Lagrangian multipliers', *RAIRO Anal. Numer.*, **8**, 129–151 (1974).
13. M. Fortin and R. Pierre, 'On the convergence of the mixed method of Crochet and Marchal for viscoelastic flows', *Comput. Methods Appl. Mech. Eng.*, **73**, 341–350 (1989).
14. J. M. Marchal and M. J. Crochet, 'A new mixed finite element for calculating viscoelastic flow', *J. Non-Newtonian Fluid Mech.*, **26**, 77–114 (1987).
15. A. N. Brooks and T. J. R. Hughes, 'Streamline upwind/Petrov– Galerkin formulations for convection dominated flows with particular emphasis on the incompressible Navier–Stokes equations', *Comput. Methods Appl. Mech. Eng.*, **32**, 199–259 (1982).
16. X. L. Luo and R. I. Tanner, 'A decoupled finite element streamline-upwind scheme for viscoelastic flow problems', *J. Non-Newtonian Fluid Mech.*, **31**, 143–162 (1989).
17. R. I. Tanner and H. Jin, 'A study of some numerical viscoelastic schemes', *J. Non-Newtonian Fluid Mech.*, **41**, 171–196 (1991).
18. M. Fortin and A. Fortin, 'A new approach for FEM simulation of viscoelastic flows', *J. Non-Newtonian Fluid Mech.*, **32**, 295 – 310 (1989).

19. A. Fortin and A. Zine, 'Computing viscoelastic fluid flow problems at low cost', *J. Non-Newtonian Fluid Mech.*, **45**, 209–229 (1992).
20. P. Lesaint and P. A. Raviart, 'On a finite element method for solving the neutron transport equation', in C. de Boor (ed.), *Mathematical Aspects of Finite Elements in Partial Differential Equations*, Academic, New York, 1974, pp. 89–123.
21. F. A. Basombrio, G. C. Buscagalia and E. A. Dari, 'Simulation of highly elastic fluid flows without additional numerical diffusivity', *J. Non-Newtonian Fluid Mech.*, **39**, 189–206 (1991).
22. F. P. T. Baaijens, 'Numerical experiments with a discontinuous Galerkin method including monotonicity enforcement on the stick–slip problem', *J. Non-Newtonian Fluid Mech.*, **51**, 141–159 (1994).
23. R. W. Thatcher, 'Locally mass-conserving Taylor–Hood elements for two- and three-dimensional flow', *Int. j. numer. methods fluids*, **11**, 341–353 (1990).
24. D. Rajagopalan, R. C. Armstrong and R. A. Brown, 'Finite element methods for calculation of steady, viscoelastic flow using constitutive equations with a Newtonian viscosity', *J. Non-Newtonian Fluid Mech.*, **36**, 159–162 (1990).
25. F. Debae, V. Legat and M. J. Crochet, 'Practical evaluation of four mixed finite element methods for viscoelastic flow', *J. Rheol.*, **38**, 421–442 (1994).
26. H. Giesekus, 'A simple constitutive equation for polymer fluids based on the concept of deformation-dependent tensorial mobility', *J. Non- Newtonian Fluid Mech.*, **11**, 69–109 (1982).
27. A. I. Leonov, 'On a class of constitutive equations for viscoelastic liquids', *J. Non-Newtonian Fluid Mech.*, **25**, 1–59 (1987).
28. R. R. Rao and B. A. Finlayson, 'Viscoelastic flow simulation using cubic stress finite elements', *J. Non-Newtonian Fluid Mech.*, **43**, 61–82 (1992).
29. R. Y. Chang and W. L. Yang, 'Numerical simulation of non-isothermal extrudate swell at high extrusion rates', *J. Non-Newtonian Fluid Mech.*, **51**, 1–19 (1994).
30. J. A. Nelder and R. Mead, 'Simplex method for function minimization', *Comput. J.*, **7**, 308–313 (1965).
31. A. I. Leonov, E. H. Lipkina, E. D. Pashkin and A. N. Prokunin, 'Theoretical and experimental investigation of shearing in elastic polymeric liquids', *Rheol. Acta*, **15**, 411–426 (1976).
32. Y. H. Huang and A. I. Isayev, 'An experimental study of planar entry flow of rubber compound', *Rheol. Acta*, **32**, 270–276 (1993).
33. C. A. Hieber, in A. I. Isayev (ed.), *Injection and Compression Molding Fundamentals*, Marcel Dekker, New York, 1987, Chap. 1.
34. W. Pfandl, G. Link and F. R. Schwarzl, 'Dynamic shear properties of a technical polystyrene melt', *Rheol. Acta*, **23**, 277–290 (1984).
35. R. G. Larson, 'Elongational-flow predictions of the Leonov constitutive equation', *Rheol. Acta*, **22**, 435–448 (1984).
36. R. K. Upadhyay and A. I. Isayev, 'Elongational flow behavior of polymeric fluids according to the Leonov model', *Rheol. Acta*, **22**, 557–568 (1983).
37. R. K. Upadhyay and A. I. Isayev, 'Nonisothermal elongational flow of polymeric fluids according to the Leonov model', *J. Rheol.*, **28**, 581–599 (1984).